ARTICLE

Unique Synthesis of Few-Layer Graphene Films on Carbon-Doped $Pt_{83}Rh_{17}$ Surfaces

Jian-Hua Gao,[†,*] Daisuke Fujita,[†,‡,*] Ming-Sheng Xu,[§] Keiko Onishi,[†] and Satoru Miyamoto[∥]

[†]Advanced Nano Characterization Center, [‡]International Center for Materials Nanoarchitectonics, [§]and International Center for Young Scientists, National Institute for Materials Science, 1-2-1 Sengen, Tsukuba, Ibaraki 305-0047, Japan, and [∥]Rockgate Company, Hongo 1-11-12, Bunkyo-Ku, Tokyo 113-0033, Japan

ABSTRACT We report a unique synthesis of single- and few-layer graphene films on carbon-doped $Pt_{83}Rh_{17}$ surfaces by surface segregation and precipitation. The ultrathin graphene films were characterized by atomic force microscopy, Auger electron spectroscopy, and micro-Raman spectroscopy measurements, providing evidence of graphene film thickness and structural quality. The G and 2D band intensity images from micro-Raman spectroscopy measurements confirm that the graphene films with different coverage have very limited defects. Additionally, the 2D band peak can be well-fitted by a single Lozentian peak, indicating that graphene films are characteristic of single layer graphene. Graphene film thickness can be determined by analysis of Auger spectra, indicating that graphene films after 850 °C annealing mainly consist of monolayer graphene. By precise adjustment of annealing temperature, graphene film thickness and area size can be controlled and uniform large-area single-layer and double-layer graphene can be achieved.

KEYWORDS: graphene · synthesis · atomic force microscopy · Raman spectroscopy · Auger electron spectroscopy

Graphene, a single layer of sp^2-bonded carbon atoms arranged into a two-dimensional honeycomb lattice, has attracted the interests of many researchers, due to its unique properties including an anomalous integer quantum Hall effect,[1−4] quantum confinement in nanoscale ribbons,[5] and long-range ballistic transport at room temperature.[6] Recently, much progress has been achieved for fabrication of graphene films. However, the fabrication of large-area, high-quality graphene films remains a challenge, and each method has limitations. Graphene sheets prepared by micromechanical exfoliation from highly oriented pyrolytic graphite (HOPG)[7] have high crystalline quality but are limited to small dimensions and are difficult to scale up for applications. Thermal decomposition of silicon carbide (SiC)[8−11] has yet to show success in achieving large graphene domains with uniform thickness. Chemical vapor deposition (CVD)[12−14] of hydrocarbons on metal surfaces can produce graphitic layers, but a large amount of carbon absorbed on the surfaces usually results in thick graphene films.[15] Epitaxial growth of graphene has been performed on single transition metal surfaces such as Ru(0001)[16−18] and Ir(111)[19,20] surfaces. These findings have led to high-quality single-crystalline graphene systems, which can be used for further fundamental research.

Here we develop a unique technique to fabricate few-layer graphene films on transition metal surfaces such as Pt, Pd, Co, Ni, and their alloys. It is known that 3-D growth of graphitic carbon occurs on carbon-doped metal surfaces at elevated temperatures by a surface segregation and precipitation process.[21−23] Using this technique, monolayer and multilayer graphitic structures on metal surfaces have previously been successfully fabricated by Fujita *et al.*[24,25] They also discovered that few-layer graphenes together with carbon nanowires can be formed on C-doped Ni(111) surfaces.[26] In this work, by ultrahigh vacuum (UHV) annealing of carbon-doped polycrystalline $Pt_{83}Rh_{17}$ surfaces, controllable single- and few-layer graphene films have been successfully prepared. We combine atomic force microscopy (AFM), micro-Raman spectroscopy, and Auger electron spectroscopy (AES) measurements to investigate the graphene films grown on $Pt_{83}Rh_{17}$ surfaces. From micro-Raman spectroscopy measurements, strongly defect-suppressed graphene films with few layers have been confirmed. Also, according to the intensity ratios of C KLL and Pt NOO peaks from the AES differential spectra, the amount of carbon is estimated and the thickness of the graphene films is determined, showing that the graphene growth changes from graphene domains to single- and few-layer graphene films. Furthermore, by precise ad-

*Address correspondence to gao.jian-hua@nims.go.jp, fu-jita.daisuke@nims.go.jp.

Received for review September 19, 2009 and accepted January 14, 2010.

Published online January 27, 2010. 10.1021/nn901255u

justment of annealing temperature, large-area single- and few-layer graphene films are achieved. Therefore, the present synthesis can fabricate well-controlled graphene films in thickness and lateral dimensions, which provides a novel technique for large-scale graphene fabrication used for further fundamental research as well as device integration.

RESULTS AND DISCUSSION

Topography and phase images were obtained by intermittent contact mode AFM for both $Pt_{83}Rh_{17}$ surfaces and graphene on the $Pt_{83}Rh_{17}$ surfaces. Figure 1 shows topography (A) and phase (B) images for clean $Pt_{83}Rh_{17}$ surfaces obtained by annealing at 1100 °C for 10 min, in which clear steps and terraces are visible. The height of the steps varies from 5 to 10 nm, depending on the orientation of the crystalline grains. Since the phase image is not affected by large-scale height difference, it provides more clear observation of step edges. Figure 1C,D presents topography and phase images of graphene films grown on $Pt_{83}Rh_{17}$ surfaces by annealing at 850 °C for 10 min. Both topography and phase images reveal obvious different features. Steps are still visible in some regions, and we believe that these regions are not covered by graphene. A region in which steps are no longer visible is evidence of a graphene layer formed on the surface. In the stepped regions, the steps in (D) are dulled compared to those in (B), and we can conclude that, even in the areas with no graphene growth, carbon atoms or clusters have segregated to the surface and nucleated at the edge of steps. In spite of these stepped regions, there is a very flat region (area indicated by a) of single-layer graphene (evidenced by AES measurements in the following section). On the top of single-layer graphene, there exists several small areas exhibiting light contrast in the phase image (D) (not so apparent in the topography image (C)). These should be additional small graphene domains where nucleation has occurred. Height measurements extracted from the topography image show that the thicknesses of these small-area graphene domains are either 0.38 nm (indicated by arrow b) or 0.82 nm (indicated by arrow c), corresponding to the height of single- and double-layer graphene domains, respectively. The graphene films are continuous, running across the steps within the same grain area. Nevertheless, because of the polycrystallinity of the $Pt_{83}Rh_{17}$ surfaces, graphene films become discontinuous at the grain boundaries of the surfaces. We also observe a carbon nanowire (indicated by d) floating on the top of the stepped areas. This was previously reported for the Ni(111) case.[26]

The thermal processing of carbon-doped surfaces controls the amount of carbon that precipitates to the surfaces during graphene growth. In order to determine the carbon concentration in surface layers, scanning Auger microscopy (SAM) was used to investigate the

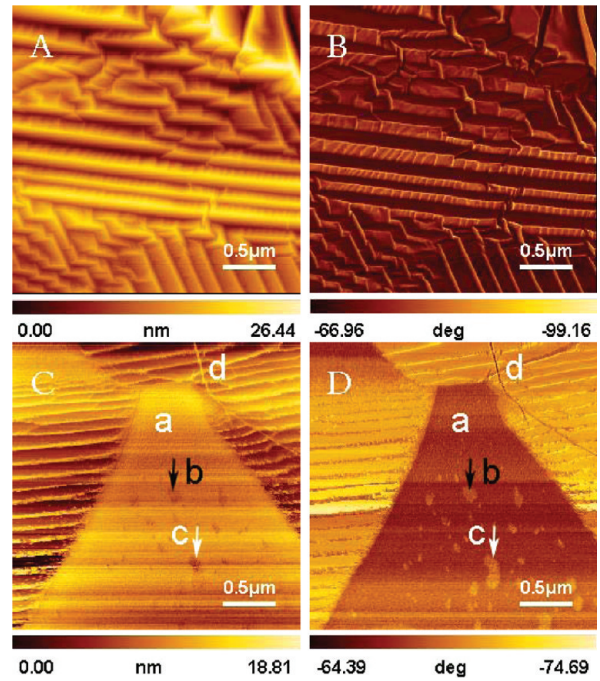

Figure 1. AFM images acquired by intermittent contact mode at room temperature for graphene films grown on the $Pt_{83}Rh_{17}$ surfaces. Topography (A) and phase (B) images of clean $Pt_{83}Rh_{17}$ surfaces after high-temperature annealing. Steps and terraces can be clearly visible. Topography (C) and phase (D) images of graphene films grown on the $Pt_{83}Rh_{17}$ surfaces anneled at 850 °C for 10 min. In some regions, steps are still visible but dulled compared with those in (A) and (B), which is due to the carbon atoms or cluster segregation to the surfaces. A very flat region corresponds to the monolayer graphene covered region with new small graphene nucleation on the top.

graphene films on $Pt_{83}Rh_{17}$ surfaces. Figure 2A shows a scanning electron microscopy (SEM) image of the graphene films obtained by annealing at 850 °C for 10 min. Figure 2B presents C KLL mapping image with the same area as that of the SEM image. From the C KLL image, discrete color contrasts are visible, indicating discrete intensity of carbon Auger signals in the mapping images. The variation in carbon intensity represents graphene films with different coverage. The AES differential spectra corresponding to dark, red, and light yellow areas in the C KLL map are shown in Figure 2C. It can be seen that, for the darkest area (indicated by arrow a), the spectrum exhibits the highest Pt NOO peak and weakest C KLL peak, whereas for the spectrum corresponding to the red color region (indicated by arrow b), the carbon peak becomes stronger and the platinum peak becomes weaker. The spectrum corresponding to the light yellow color area (indicated by arrow c) displays an more prominent carbon peak and a decreased platinum peak. According to the intensity ratios of C KLL and Pt NOO peaks in the differential spectra, the carbon concentration in each layer can be estimated. The C KLL and Pt NOO peak intensities are normalized by $\bar{I}_C = I_C/S_C$ and $\bar{I}_{Pt} = I_{Pt}/S_{Pt}$, where I_C and I_{Pt} are the peak−peak magnitudes in the differential spectra, S_C

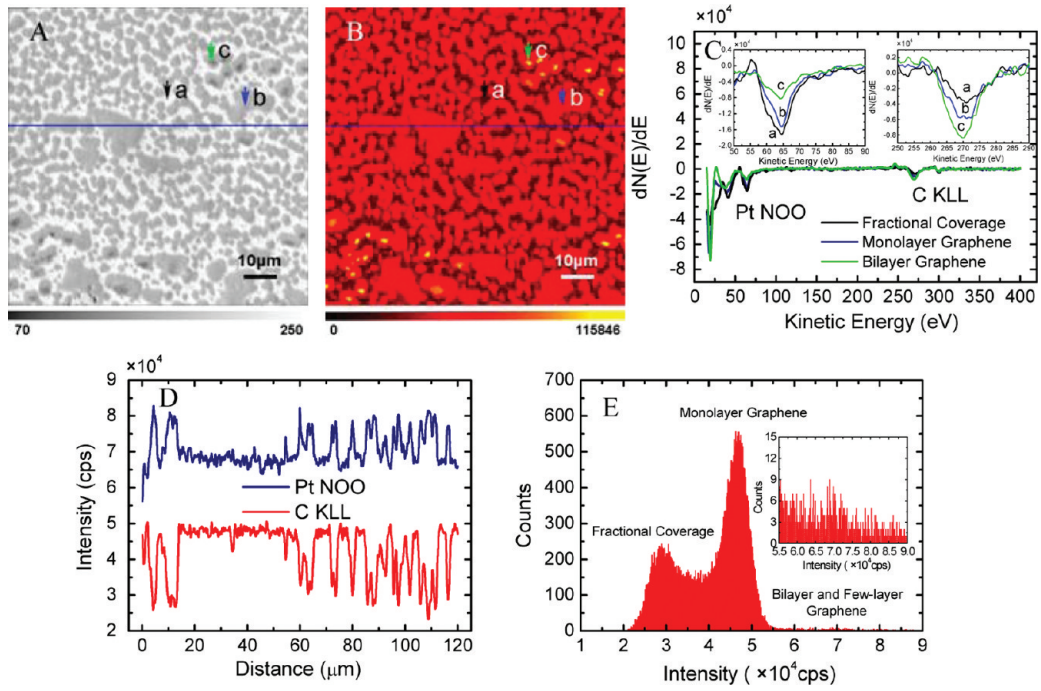

Figure 2. Scanning Auger spectroscopy characterization of the graphene films grown on the $Pt_{83}Rh_{17}$ surfaces annealed at 850 °C. Scanning electron microscopy (A), C KLL (B) mapping image with the same area. Auger differential spectra (C) with different contrast areas indicated by arrows in (A) and (B). The cross-sectional line profile (D) along the line indicated in the C KLL map. Histogram (E) of the graphene films with different coverage, indicating that monolayer graphene is dominant.

and S_{Pt} are the relative sensitivity factors.[27] Therefore, the total carbon concentration is

$$\bar{P}_C = \frac{\bar{I}_C}{\bar{I}_C + \bar{I}_{Pt}} \quad (1)$$

On the other hand, Auger signals are collected from the topmost several surface layers, the signal intensity I_d of each element decays exponentially as the distance d from the surface and is given by[28]

$$I_d = I_0 \exp(-d/\lambda \sin \alpha) \quad (2)$$

here I_0 is the intensity without inelastic attenuation, d is interplanar distance (~2.25 Å for platinum and ~3.4 Å for graphite); λ is the inelastic mean free path of Auger electrons, which is approximated to be 7.0 and 4.3 Å for C KLL and Pt NOO electrons, respectively;[29,30] α is the electron takeoff angle (~47.7°) during the Auger measurements.[27] Considering the exponential decay dependence on the distance d, the contribution of C KLL and Pt NOO signal from different layers is expressed as[31]

$$\bar{I}_C = \sum_n P_C^n \exp[-(n-1)d_C/\lambda_{C\,KLL} \sin \alpha] \quad (3)$$

$$\bar{I}_{Pt} = \sum_n P_{Pt}^n \exp[-(n-1)d_{Pt}/\lambda_{Pt\,NOO} \sin \alpha] \quad (4)$$

where P_C^n and P_{Pt}^n are the carbon and platinum concentrations in each layer and n is the number of layers. Using eqs 1−4, the carbon concentration in each layer can be calculated for different color regions. During the calculation, the following model was assumed on the basis of our experimental results.

1. When graphene coverage is less than 1.0 ML, we assume that all C KLL signal comes from the first layer because carbon signal from the internal should be very small due to the low carbon concentration (~0.5%). As for the Pt NOO signal, except the contribution of the first layer, from the second layer, the contribution is the same as the bulk $Pt_{83}Rh_{17}$ alloy. Using the above assumption, for the darkest area (C KLL map), the carbon concentration of the top layer ($n = 1$) is estimated about 67.2%, which means that the carbon coverage is around 0.67 ML. We can regard it as fractional graphene coverage, consisting of segregated carbon atoms. For the red color area (C KLL map), according to the above assumption, the carbon concentration in the first layer ($n = 1$) is calculated as about 110.8%. Despite there being a carbon concentration error about 10%, we can regard this as monolayer graphene.
2. For the yellow color area (C KLL map), the carbon atoms are segregated not only to the first layer but also to the second layer ($n = 2$). We assume that all C KLL signal comes from the top two layers. For the Pt NOO signal, from the third layer, the contribution is the same as the bulk $Pt_{83}Rh_{17}$ alloy. Using this assumption, the carbon concentration is calculated as 105. 1%, roughly corresponding to bilayer of graphene.

Therefore, by analyzing the AES spectra, we can determine the graphene thickness, indicating that graphene after annealing at 850 °C consists of less than a few layers, and monolayer graphene appears to be dominant. Figure 2D is the line profile for the C KLL and Pt NOO peaks. There exists a clear complementarity between the C KLL and Pt NOO intensity. It is clear that, for both carbon and platinum, the intensity signal is separated into two discrete values (8.2×10^4 and 6.8×10^4 cps for the Pt NOO signal; 2.8×10^4 and 4.7×10^4 cps for the C KLL signal), indicating that intensity varies from fractional graphene coverage to monolayer graphene. Figure 2E is the statistics histogram from the C KLL image (B), in which two dominant peaks with the intensities of 2.8×10^4 and 4.7×10^4 cps are observed, corresponding to fractional graphene coverage and monolayer graphene, respectively. The inset is the distribution for bilayer graphene, and the count number is much lower than that of monolayer graphene. Further analysis indicates that more than 70% of the area is covered with single-layer graphene. Fractional graphene coverage area is about 28%, and the rest is double- and few-layer graphene (less than 2%). The growth mechanism for graphene on carbon-doped $Pt_{83}Rh_{17}$ surfaces partially follows the Stranski−Krastanov growth mode, based on the surface precipitation process of doped carbon, similar to the Ni(111) case.[24−26]

Since the surface segregation process is closely related to the annealing temperature, we annealed the carbon-doped $Pt_{83}Rh_{17}$ surfaces at different temperatures in order to optimize the growth of graphene. Figure 3 presents the C KLL mapping images annealing at different temperatures from 900 to 1150 °C. Figure 3A shows the C KLL map image after annealing at 900 °C for 10 s. By using the above method, we calculated the graphene thickness for different color contrasts. Carbon coverage for the dark red color area (indicated by a) is 0.85 ML, and the red color area (indicated by b) is identified as a single layer (carbon concentration is 98.7%). The light yellow area (indicated by c) represents bilayer graphene (carbon concentration is 96.4%), and the white yellow area (indicated by d) is assigned to be trilayer graphene (carbon concentration is 98.6%). Compared to that annealed at 850 °C, the domain sizes are much larger. Figure 3B−F presents the C KLL images annealing at 950, 1000, 1050, 1100, and 1150 °C for 10 s, respectively. After annealing above 950 °C, uniform single-layer (I area) or double-layer (II area) graphene films are obtained on $Pt_{83}Rh_{17}$ surfaces, resulting in macroscopic graphene domains reaching over 100 μm in size, much larger than that previously reported.[20,32] Our findings indicate that, by annealing below 900 °C, coexistence of fractional graphene coverage, monolayer graphene and bilayer graphene can be obtained. Uniform single-layer and double-layer graphene film can be stabilized between 950 and 1150 °C, except some extra small area at the boundary between different crystalline grains, there exists some multilayer graphene. Therefore, by our technique, the number of graphene layers and graphene domain size can be controlled by optimizing the annealing temperature and cooling down speed during the segregration process.

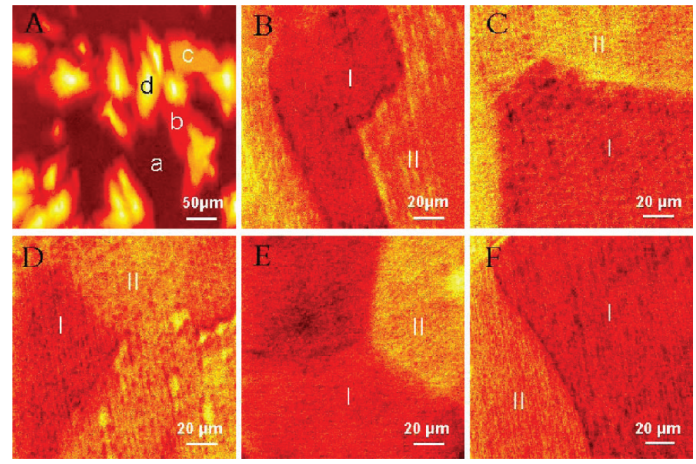

Figure 3. Scanning Auger spectroscopy characterization of the graphene films grown on the $Pt_{83}Rh_{17}$ surfaces after annealing at different temperatures. C KLL images (A−F) after annealing at 900, 950, 1000, 1050, 1100, and 1150 °C for 10 s, indicating that large-area single- and double-layer graphene can be obtained.

Raman spectroscopy is a widely used technique to characterize the structural and electronic properties of carbon-based materials such as carbon nanotubes, graphite, and graphene.[33−43] The recent discovery of clear signatures in graphene makes it a powerful method to determine the number of layers in few-layer graphene films.[12,44,45] According to previous studies, there are several prominent peaks in the spectrum. The D band peak appears around 1350 cm^{-1}, and its signal strength relative to G band is strongly dependent on the amount of disorder in graphene. The G band appears at ~1580 cm^{-1} due to the two-fold degenerate E_{2g} mode at the zone center, and a second-order 2D band is present at ~2700 cm^{-1} due to the highest optical branch phonons near K point at the Brillouin zone boundary.[45] To further evaluate the quality and verify the thickness for graphene films grown on the $Pt_{83}Rh_{17}$ surfaces, spatially resolved Raman spectroscopy has been carried out. Figure 4 summarizes micro-Raman experiments at 532 nm excitation for graphene films, providing information on the quality and thickness of the graphene films. Figure 4A is the mapping image of the G band intensity integrated from 1533 to 1622 cm^{-1} and (B) is the 2D band intensity integrated from 2644 to 2726 cm^{-1}. Both the G band and the 2D band images show color contrasts between single- and double-layer graphene, with the brighter region corresponding to thicker coverage. Figure 4C shows typical Raman spectra for different color regions indicated in Figure 4A. The spectra exhibit dominant peaks at G band (1583 cm^{-1}) and 2D band (2696 cm^{-1}) frequencies. The appearance of the D band (1350 cm^{-1}) is related to defects, and in

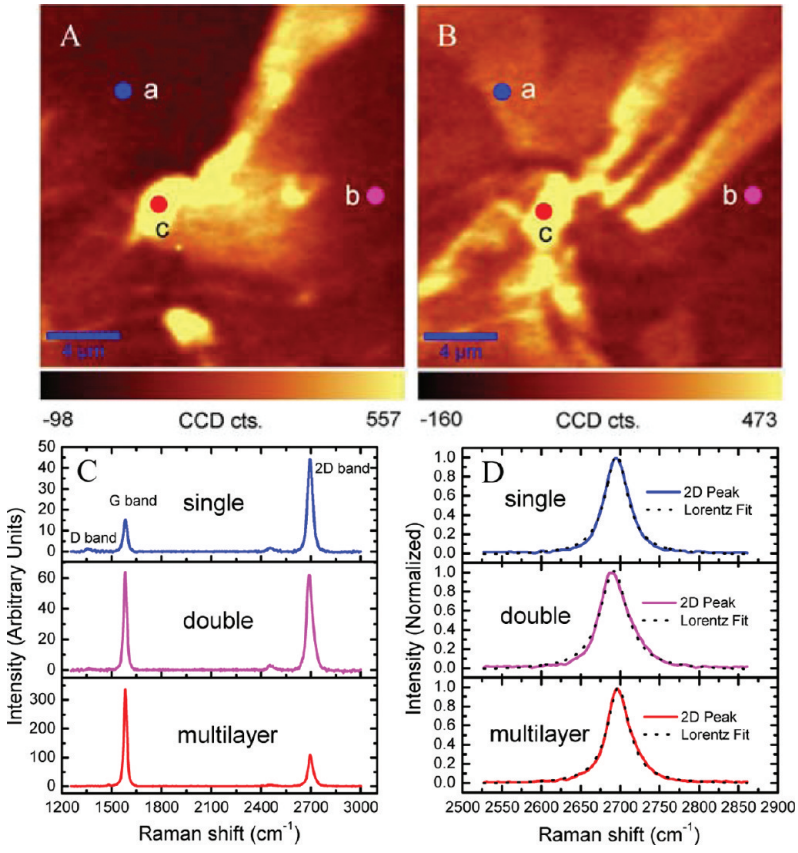

Figure 4. Raman imaging and spectra of the graphene films on the $Pt_{83}Rh_{17}$ surfaces. Intensity mapping images of the G band integrated from 1544 to 1622 cm^{-1} (A) and the 2D band integrated from 2644 to 2726 cm^{-1} (B). Raman spectra (C) corresponding to the marked solid circle (a), (b), and (c) indicated in (A), showing the presence of single, double, and multilayer of graphene films. Normalized 2D band peaks (D) with single, double, and multilayer of graphene; the dotted line is fitted by a single Lorentz curve.

our samples, it is very weak for single-layer graphene and almost not observed for double and multilayer graphene. The strongly suppressed defect-related D band peaks indicate overall good quality of our graphene films. Furthermore, it can be seen that Raman spectra features with different numbers of layers are distinctly different, with different intensity ratio between G band and 2D band. It has been reported that the G to 2D peak intensity ratio can provide a method for fast estimation of the number of graphene layers.[12,44] For the area marked by solid circle (a), the intensity of the 2D band peak is much stronger than that of G band, and the G to 2D peak intensity ratio of 0.3 is observed, corresponding to single-layer graphene. The intensity of G and 2D band peaks in the region (b) is comparable, with the G to 2D ratio close to 1.0, representing bilayer graphene. The G to 2D band peak ratios of 0.3 and 1.0 correspond to single- and double-layer graphene, respectively, which is consistent with graphene grown on Ni surfaces by CVD method.[12] Furthermore, for the typical Raman spectrum of multilayer graphene (indicated by solid circle c), the G band intensity is much stronger compared to that of the 2D band peak. In addition, for the case of HOPG-exfoliated graphene, 2D peak shape can be used to distinguish between single- and double-layer graphene, with a sharp and symmetric single Lorentzian 2D peak for single-layer graphene. For double-layer graphene films, the 2D band peak is resolved into two or more components because of degenerate electronic bands. However, in our graphene formed on the carbon-doped metal substrate, we observe that all of the spectra exhibit a symmetric and sharp peak with the line width of 36−40 cm^{-1} at the position of 2686−2696 cm^{-1}. The 2D peaks with different thickness can be well fitted by a single Lorentzian curve shown in Figure 4D, being characteristic of single-layer graphene. According to previous reports,[12] for order stacked bilayer graphene, the strong interaction between the two layers splits the degenerate electronic structure bands, giving rise to four Lorentzian components in the 2D peak. For non-order stacked structures, the interactions between the two layers are weak and the 2D peak remains a single Lorentzian peak. Hass *et al.*,[46] by using first principle calculation, have confirmed that the stacking faults decouple adjacent graphene sheets, so that the linear dispersion at the K point still is preserved even though the films are composed of many graphene sheets. Accordingly, the band structure of multilayer graphene is maintained to be identical with that of the isolated graphene. Therefore, a single Lorentzian peak indicates that graphene films exhibit an non-ordered stacking and absence of electronic coupling between graphene layers, so our multilayer graphene should have electronic properties similar to that of single-layer graphene.

CONCLUSION

In summary, controllable, uniform, continuous single- and few-layer graphene film has been fabricated by thermal treatments of the carbon-doped metal surfaces. By using AFM, AES, and Raman spectroscopy, it is confirmed that graphene films with different coverage have been successfully obtained. The films exhibit that a large percentage of single-layer graphene regions with the lateral size can be controlled by adjusting the annealing temperature. This approach enables an alternative route toward mass production of graphene films for future applications.

EXPERIMENTAL SECTION

The few-layer graphene films were prepared by surface segregation and precipitation process on carbon-doped $Pt_{83}Rh_{17}$ surfaces. A high purity (99.99%) polycrystalline $Pt_{83}Rh_{17}$ sheet with the size of 10×10 mm^2 and thickness of 0.1 mm was used as the starting material. Doping with carbon was performed by solid-state diffusion method. The $Pt_{83}Rh_{17}$ sheet was covered with high purity graphite powder and kept at 800 °C in a high vacuum chamber for 48 h. Carbon atoms from the powder dissolve into the $Pt_{83}Rh_{17}$ surfaces until solid solution equilibrium is established. This equilibrium state depends on carbon solubility in platinum, and the atomic concentration was estimated to be about 0.5% according to the Pt−C phase diagram.[47] The $Pt_{83}Rh_{17}$ surfaces doped with carbon were introduced into the UHV chamber and heated to high temperature by electron back-bombardment. Since the solubility of carbon in the metal is temperature-dependent, during the annealing process, carbon atoms precipitate to the surface as a graphene layer upon cooling of the sample.

AES measurements were performed at room temperature with a scanning Auger microscope (ULVAC-PHI model SAM650) with a cylindrical mirror analyzer. AES spectra were recorded with a primary electron beam of 5.0 kV. Differential $dN(E)/dE$ Auger spectra were obtained by numerical derivation of raw $N(E)$ integrated Auger data by Savitzky−Golay differential filter using 5 points. The differential spectra were used to estimate the carbon concentration in each layer, and the coverage of the graphene films was determined. The identity and thickness of the graphene films were also determined by AFM and micro-Raman spectroscopy measurements. The AFM images were acquired by intermittent contact mode (SPA 400, SII Nanotechnology, Japan) at room temperature. We used a Si cantilever (SI-DF20S) with resonance frequency of about 127 kHz and force constant of about 12 N/m. The tips were checked by characterization of standard anodic porous film, and details were discussed elsewhere.[48] Raman mapping images and spectra were recorded by a conformal laser Raman microscope (WITec alpha300R) at room temperature. The Ar ion laser of 532 nm was used as the excitation source with the laser power 50 mW. The spatial resolution is 360 nm, and the spectral resolution is 3.0 cm^{-1}.

Acknowledgment. The authors especially appreciate fruitful discussion with K. Sagisaka and Y.H. Yu and generous assistance in English from J. Stiver. This work was in part supported by World Premier International Research Center (WPI) Initiative on Materials Nanoarchitectonics, MEXT, Japan.

REFERENCES AND NOTES

1. Geim, A. K.; Novoselov, K. S. The Rise of Graphene. *Nat. Mater.* **2007**, *6*, 183–191.
2. Novoselov, K. S.; Geim, A. K.; Morozov, S. V.; Jiang, D.; Katsnelson, M. I.; Grigorieva, I. V.; Dubonos, S. V.; Firsov, A. A. Two-Dimensional Gas of Massless Dirac Fermions in Graphene. *Nature* **2005**, *438*, 197–200.
3. Zhang, Y. B.; Tan, Y. W.; Stormer, H. L.; Kim, P. Experimental Observation of the Quantum Hall Effect and Berry's Phase in Graphene. *Nature* **2005**, *438*, 201–204.
4. Novoselov, K. S.; McCann, E.; Morozov, S. V.; Falḱo, V. I.; Katsnelson, M. I.; Zeitler, U.; Jiang, D.; Schedin, F.; Geim, A. K. Unconventional Quantum Hall Effect and Berry's Phase of 2π in Bilayer Graphene. *Nat. Phys.* **2006**, *2*, 177–180.
5. Berger, C.; Song, Z. M.; Li, X. B.; Wu, X. S.; Brown, N.; Naud, C.; Mayou, D.; Li, T. B.; Hass, J.; Marchenkov, A. N. Electronic Confinement and Coherence in Patterned Epitaxial Graphene. *Science* **2006**, *312*, 1191–1196.
6. Novoselov, K. S.; Jiang, Z.; Zhang, Y.; Morozov, S. V.; Stormer, H. L.; Zeitler, U.; Maan, J. C.; Boebinger, G. S.; Kim, P.; Geim, A. K. Room-Temperature Quantum Hall Effect in Graphene. *Science* **2007**, *315*, 1379.
7. Novoselov, K. S.; Geim, A. K.; Morozov, S. V.; Jiang, D.; Zhang, Y.; Dubonos, S. V.; Grigorieva, I. V.; Firsov, A. A. Electric Field Effect in Atomically Thin Carbon Films. *Science* **2004**, *306*, 666–669.
8. Rutter, G. M.; Crain, J. N.; Guisinger, N. P.; Li, T.; First, P. N.; Stroscio, J. A. Scattering and Interference in Epitaxial Graphene. *Science* **2007**, *317*, 219–222.
9. Guisinger, N. P.; Rutter, G. M.; Crain, J. N.; First, P. N.; Stroscio, J. A. Exposure of Epitaxial Graphene on SiC(0001) to Atomic Hydrogen. *Nano Lett.* **2009**, *9*, 1462–1466.
10. Miller, D. L.; Kubista, K. D.; Rutter, G. M.; Ruan, M.; Heer, W. A.; First, P. N.; Stroscio, J. A. Observing the Quantization of Zero Mass Carriers in Graphene. *Science* **2009**, *324*, 924–927.
11. Heer, W. A.; Berger, C.; Wu, X. S.; First, P. N.; Conrad, E. H.; Li, X. B.; Li, T. B.; Sprinkle, M.; Hass, J.; Sadowski, M. L.; *et al.* Epitaxial Graphene. *Solid State Commun.* **2007**, *143*, 92–100.
12. Reina, A.; Jia, X. T.; Ho, J.; Nezich, D.; Son, H. B.; Bulovic, V.; Dresselhaus, M. S.; Kong, J. Large Area, Few-Layer Graphene Films on Arbitrary Substrates by Chemical Vapor Deposition. *Nano Lett.* **2009**, *9*, 30–35.
13. Li, X. S.; Cai, W. W.; An, J. H.; Kim, S. Y.; Nah, J.; Yang, D. X.; Piner, R.; Velamakanni, A.; Jung, I.; Tutuc, E. Large-Area Synthesis of High-Quality and Uniform Graphene Films on Copper Foils. *Science* **2009**, *324*, 1312–1314.
14. Kim, K. S.; Zhao, Y.; Jang, H.; Lee, S. Y.; Kim, J. M.; Kim, K. S.; Ahn, J. H.; Kim, P.; Choi, J. Y.; Hong, B. H. Large-Scale Pattern Growth of Graphene Films for Stretchable Transparent Electrodes. *Nature* **2009**, *457*, 706–710.
15. Obraztsov, A. N.; Obraztsova, E. A.; Tyurnina, A. V.; Zolotukhin, A. A. Chemical Vapor Deposition of Thin Graphite Films of Nanometer Thickness. *Carbon* **2007**, *45*, 2017–2021.
16. Sutter, P. W.; Flege, J. I.; Sutter, E. A. Epitaxial Graphene on Ruthenium. *Nat. Mater.* **2008**, *7*, 406–411.
17. Sutter, P. W.; Hybertsen, M. S.; Sadowski, J. T.; Sutter, E. A. Electronic Structure of Few-Layer Epitaxial Graphene on Ru(0001). *Nano Lett.* **2009**, *9*, 2654–2660.
18. Pan, Y.; Zhang, H. G.; Shi, D. X.; Sun, J. T.; Du, S. X.; Liu, F.; Gao, H. J. Highly Ordered, Millimeter-Scale, Continuous, Single-Crystalline Graphene Monolayer Formed on Ru(0001). *Adv. Mater.* **2008**, *20*, 1–4.
19. Pletikosić, I.; Kralj, M.; Pervan, P.; Brako, R.; Coraux, J.; N'Diaye, N.; Busse, A. T.; Michely, T. Dirac Cones and Minigaps for Graphene on Ir(111). *Phys. Rev. Lett.* **2009**, *102*, 056808/1–056808/4.
20. Coraux, J.; N'Diaye, N.; Busse, A. T.; Michely, T. Structural Coherency of Graphene on Ir(111). *Nano Lett.* **2008**, *8*, 565–570.
21. Eizenberg, M.; Blakely, J. M. Carbon Monolayer Phase Condensation on Ni(111). *Surf. Sci.* **1979**, *82*, 228–236.
22. Eizenberg, M.; Blakely, J. M. Carbon Interaction with Nickel Surfaces: Monolayer Formation and Structural Stability. *J. Chem. Phys.* **1979**, *71*, 3467–3477.
23. Hamilton, J. C.; Blakely, J. M. Carbon Segregation to Single Crystal Surfaces of Pt, Pd and Co. *Surf. Sci.* **1980**, *91*, 199–217.
24. Fujita, D.; Yoshihara, K. Surface Precipitation Process of Epitaxially Grown Graphite (0001) Layers on Carbon-Doped Nickel(111) Surface. *J. Vac. Sci. Technol., A* **1994**, *12*, 2134–2139.
25. Fujita, D.; Schleberger, M.; Tougaard, S. XPS Study of the Surface Enrichment Process of Carbon on C-doped Ni(111) Using Inelastic Background Analysis. *Surf. Sci.* **1995**, *331−333*, 343–348.
26. Fujita, D.; Kumakura, T.; Onishi, K.; Sagisaka, K.; Ohgi, T.; Harada, M. Sprout-like Growth of Carbon Nanowires on a Carbon-Doped Ni(111) Surface. *Surf. Sci.* **2004**, *566*, 361–366.
27. *Handbook of Auger Electron Spectroscopy*; Physical Elecronics: Eden Prairie, MN, 1995.
28. Briggs D.; Seah M. P. *Practical Surface Analysis by Auger and X-ray Photoelectron Spectroscopy*; John Wiley: New York, 1984.
29. Tanuma, S.; Powell, C. J.; Penn, D. R. Calculations of Electron Inelastic Mean Free Paths. *Surf. Interface Anal.* **2004**, *36*, 1–14.

30. Tanuma, S.; Powell, C. J.; Penn, D. R. Calculations of Electron Inelastic Mean Free Paths. *Surf. Interface Anal.* **1991**, *17*, 911–926.
31. Yu, Y. H.; Sagisaka, K.; Fujita, D. Surface Segregation of Aluminum Atoms on Cu-9 at. % Al(111) Studied by Auger Electron Spectroscopy and Low Energy Electron Diffraction. *Surf. Sci.* **2009**, *603*, 723–726.
32. Vazquez de Parga, A. L.; Calleja, F.; Borca, B.; Passeggi, M. C. G.; Hinarejos, J. J.; Guinea, F.; Miranda, R. Periodically Rippled Graphene: Growth and Spatially Resolved Electronic Structure. *Phys. Rev. Lett.* **2008**, *100*, 056807/1–056807/4.
33. Jiao, L. Y.; Zhang, L.; Wang, X. R.; Diankov, G.; Dai, H. J. Narrow Graphene Nanoribbons from Carbon Nanotubes. *Nature* **2009**, *458*, 877–880.
34. Ferrari, A. C.; Meyer, J. C.; Scardaci, V.; Casiraghi, C.; Lazzeri, C.; Mauri, F.; Piscanec, S.; Jiang, D.; Novoselov, K. S.; Roth, S.; *et al.* Raman Spectrum of Graphene and Graphene Layers. *Phys. Rev. Lett.* **2006**, *97*, 187401/1–187401/4.
35. Ikeda, K.; Uosaki, K. Coherent Phonon Dynamics in Single-Walled Carbon Nanotubes Studied by Time-Frequency Two-Dimensional Coherent Anti-Stokes Raman Scattering Spectroscopy. *Nano Lett.* **2009**, *9*, 1378–1381.
36. Casiraghi, C.; Hartschuh, A.; Qian, H.; Piscanec, S.; Georgi, C.; Fasoli, A.; Novoselov, K. S.; Basko, D. M.; Ferrari, A. C. Raman Spectroscopy of Graphene Edges. *Nano Lett.* **2009**, *9*, 1433–1441.
37. Puech, P.; Anwar, A. W.; Flahaut, E.; Dunstan, D. J.; Bassil, A.; Bacsa, W. Raman G and D Band in Strongly Photoexcited Carbon Nanotubes. *Phys. Rev. B* **2007**, *79*, 085418/1–085418/4.
38. Picher, M.; Anglaret, E.; Arenal, R.; Jourdain, V. Self-Deactivation of Single-Walled Carbon Nanotube Growth Studied by *In Situ* Raman Measurements. *Nano Lett.* **2009**, *9*, 542–547.
39. Ni, Z. H.; Chen, W.; Fan, X. F.; Kuo, J. L.; Yu, T.; Wee, A. T. S.; Shen, Z. X. Raman Spectroscopy of Epitaxial Graphene on a SiC Substrate. *Phys. Rev. B* **2008**, *77*, 115416/1–115416/6.
40. Ni, Z. H.; Yu, T.; Lu, Y. H.; Wang, Y. Y.; Feng, Y. P.; Shen, Z. X. Uniaxial Strain on Graphene: Raman Spectroscopy Study and Band-Gap Opening. *ACS Nano* **2008**, *2*, 2301–2305.
41. Ni, Z. H.; Yu, T.; Wang, Y. Y.; Liu, L.; Wong, C. P.; Miao, J. M.; Huang, W.; Shen, Z. X. Probing Charged Impurities in Suspended Graphene Using Raman Spectroscopy. *ACS Nano* **2009**, *3*, 569–574.
42. Luo, Z. Q.; Yu, T.; Kim, K.; Ni, Z. H.; You, Y. M.; Lim, S. H.; Shen, Z. X.; Wang, S. Z.; Lin, J. Y. Thickness-Dependent Reversible Hydrogenation of Graphene Layers. *ACS Nano* **2009**, *3*, 1781–1788.
43. Ni, Z. H.; Wang, H. M.; Ma, Y.; Kasim, J.; Wu, Y. H.; Shen, Z. X. Tunable Stress and Controlled Thickness Modification in Graphene by Annealing. *ACS Nano* **2008**, *2*, 1033–1039.
44. Graf, D.; Molitor, F.; Ensslin, K.; Stampfer, C.; Jungen, A.; Hierold, C.; Wirtz, L. Spatially Resolved Raman Spectroscopy of Single- and Few-Layer Graphene. *Nano Lett.* **2007**, *7*, 238–242.
45. Gupta, A.; Chen, G.; Joshi, P.; Tadigadapa, S.; Eklund, P. C. Raman Scattering from High-Frequency Phonons in Supported *n*-Graphene Layer Films. *Nano Lett.* **2006**, *6*, 2667–2673.
46. Hass, J.; Varchon, F.; Millán-Otoya, J. E.; Sprinkle, M.; Sharma, N.; Heer, W. A.; Berger, C.; First, P. N.; Magaud, L.; Conrad, E. H. Why Multilayer Graphene on 4H-SiC(0001) Behaves Like a Single Sheet of Graphene. *Phys. Rev. Lett.* **2008**, *100*, 125504/1–125504/4.
47. http://www.asminternational.org/asmenterprise/APD/.
48. Xu, M. S.; Fujita, D.; Onishi, K. Reconstruction of Atomic Force Microscopy Image by Using Nanofabricated Tip Characterizer toward the Actual Sample Surface Topography. *Rev. Sci. Instrum.* **2009**, *80*, 043703/1–043703/6.